(submitted to Phys. Rev. B)

Metastable precursors during the oxidation of the Ru(0001) surface

Karsten Reuter[1], M.Verónica Ganduglia-Pirovano[1], Catherine Stampfl[1,2], and Matthias Scheffler[1]
[1] *Fritz-Haber-Institut der Max-Planck-Gesellschaft, Faradayweg 4-6, D-14195 Berlin, Germany*
[2] *Northwestern University, 2145 Sheridan Road, Evanston IL60208, USA*
(Received 19 September 2001)

Using density-functional theory, we predict that the oxidation of the Ru(0001) surface proceeds via the accumulation of sub-surface oxygen in two-dimensional islands between the first and second substrate layer. This leads locally to a decoupling of an O-Ru-O trilayer from the underlying metal. Continued oxidation results in the formation and stacking of more of these trilayers, which unfold into the RuO_2(110) rutile structure once a critical film thickness is exceeded. Along this oxidation pathway, we identify various metastable configurations. These are found to be rather close in energy, indicating a likely lively dynamics between them at elevated temperatures, which will affect the surface chemical and mechanical properties of the material.

I. INTRODUCTION

The interaction of metals with our oxygen-rich atmosphere leads to the oxidation of the metal surfaces. Although this is common knowledge, little is known about the *microscopic processes* that actuate this oxide formation. Roughly speaking, the reaction sequence may be divided into the initial dissociation of O_2 and O chemisorption, followed by oxide nucleation, and finally the growth of the formed oxide film. In this scheme, particularly the transition from a two-dimensional on-surface O adlayer to the three-dimensional surface-oxide nucleus has hitherto barely been addressed.

Based on a host of density-functional theory (DFT) calculations, we present an atomistic pathway for the oxide formation on the Ru(0001) surface[1]. The situation for this surface is in fact unique, as both the initial O chemisorption on the metal and the finally resulting RuO_2(110) oxide patches have already been characterized experimentally on an atomic level[2,3]. Bridging this detailed knowledge of the initial and final state of the oxidation, we predict that after the completion of a full monolayer of chemisorbed O on Ru(0001), the incorporation of O into the lattice leads to the formation of two-dimensional sub-surface O islands between the first and second substrate layer. This implies that domains are formed that have a local (1×1) periodicity and that can be described as a trilayered O_{ad}-Ru-O_{sub} film on top of Ru(0001). Further O incorporation also occurs between the first and second substrate layer, saturating the underlying metal and almost completely decoupling the O-Ru-O trilayer. The on-going oxidation results in the successive formation of more of these O-Ru-O trilayers, which at first remain in a loosely coupled stacking sequence. Once a critical film thickness is exceeded, this trilayer stack unfolds into the experimentally reported RuO_2(110) rutile structure[3].

This suggested oxidation pathway proceeds via several metastable states before the final bulk RuO_2 oxide structure is attained. Their experimental characterization would therefore provide the ultimate confirmation of our theoretical model. However, as these intermediate configurations are only metastable, their experimental identification will be challenging, requiring sophisticated choices of temperatures and pressures. Moreover, we find these structures to be very close in energy to the final bulk oxide. This points at a likely lively dynamics between these metastable configurations under realistic conditions, which might affect the chemical and mechanical properties of the surface.

II. THEORETICAL

Our DFT calculations employ the generalized gradient approximation (GGA) of the exchange-correlation functional[4], using the full-potential linear augmented plane wave method (FP-LAPW)[5–7] to solve the Kohn-Sham equations. The Ru(0001) surface is modeled using a slab with six metal layers for oxygen coverages up to two monolayers (ML) and a 10 metal layer slab for higher coverages. O is adsorbed on both sides, fully relaxing the outermost two (three) Ru layers of the six (ten) layer slabs, as well as the position of all O atoms. A vacuum region corresponding to five Ru interlayer spacings (≈11Å) is employed to decouple the surfaces of consecutive slabs in the supercell approach. The calculated geometries of the four ordered adlayers of O on Ru(0001) ($0 < \theta \leq 1$ ML) are in very good agreement with existing LEED analyses[2,8], as well as with earlier DFT pseudo-potential calculations[9,10].

The FP-LAPW basis set is taken as follows: $R_{\rm MT}^{\rm Ru}$ =2.3 bohr, $R_{\rm MT}^{\rm O}$ =1.3 bohr, wave function expansion inside the muffin tins up to $l_{\rm max}^{\rm wf} = 12$, potential expansion up to $l_{\rm max}^{\rm pot} = 4$, and local orbitals for the $4s$ and $4p$ semicore states of Ru. The Brillouin zone integration for the (1×1) cells is performed using a $(12\times12\times1)$ Monkhorst-Pack grid with 19 **k**-points in the irreducible part. For the larger surface cells, the grid is reduced accordingly, in order to obtain the same sampling of the reciprocal space. The energy cutoff for the plane wave representation in the interstitial region between the muffin tin spheres is 17 Ry

for the wave functions and 169 Ry for the potential.

The central quantity we obtain from the calculations is the average binding energy of oxygen defined as

$$E_{\rm b}(\theta) \;=\; -\frac{1}{N_{\rm O}}\;\left[\,E^{\rm slab}_{\rm cov.} - E^{\rm slab}_{\rm clean} - 1/2 N_{\rm O} E^{\rm mol.}_{\rm O_2}\,\right], \quad (1)$$

where $N_{\rm O}$ is the total number of O atoms (on- and sub-surface) present in the unit-cell at the considered coverage, θ. $E^{\rm slab}_{\rm cov.}$, $E^{\rm slab}_{\rm clean}$, and $E^{\rm mol.}_{\rm O_2}$ are the total energies of the slab containing oxygen, of the corresponding clean Ru(0001) slab, and of an isolated oxygen molecule respectively. Thus a positive binding energy, $E_{\rm b}(\theta)$, indicates that the dissociative adsorption of O_2 is exothermic.

Due to the small bond length, the total energy of the isolated O_2 molecule, $E^{\rm mol.}_{\rm O_2}$, cannot directly be calculated with the muffin tin radius, $R^{\rm O}_{\rm MT}$ =1.3 bohr, chosen for the surface calculations. Correspondingly we compute the total energy of an isolated oxygen atom with $R^{\rm O}_{\rm MT}$ =1.3 bohr inside a cubic cell of side length 15 bohrs with Γ-point sampling of the Brillouin zone without spherically averaging the electron density in the open shell. To arrive at $1/2E^{\rm mol.}_{\rm O_2}$, we then add to the atomic energy one half of the binding energy of the O_2 molecule. The latter is calculated inside the same box using oxygens with $R^{\rm O}_{\rm MT}$ =1.1 bohr, where due to the smaller muffin tin radius the kinetic-energy cutoff for the plane-wave basis needed for the interstitial region has been increased to 24 Ry[11].

The numerical accuracy of $E_{\rm b}(\theta)$ is limited by the finite FP-LAPW basis set, as well as by the finite size of slab and vacuum region in the supercell approach. To check this accuracy we selectively increased these parameters and compared the binding energies within a subset of the considered structures. This subset is formed by the two most stable of all tested geometries at each full monolayer coverage in the discussed $0 \le \theta \le 3$ ML sequence, i.e. the clean surface at $\theta = 0$ ML and the two most stable O sites at $\theta = 1, 2$ and 3 ML. As the main error is introduced by the DFT description of the atomic and molecular oxygen, a possible error cancelation will be least effective for the absolute value of the binding energy, which however is not the quantity entering our physical argument. Rather, it is the difference in binding energies of two geometries, which determines which one is more stable (if they contain the same amount of oxygen) or how $E_{\rm b}(\theta)$ evolves with coverage (if the structures contain an unequal amount of O). The accuracy will be largest in the former case, where the molecular energy entering eq. (1) completely cancels, so that we will always state two values indicating the numerical uncertainty, when comparing relative binding energies in geometries containing an equal (unequal) amount of O.

To assess the quality of the basis set, we increased the plane wave cutoff in the interstitial region from 17 Ry to 24 Ry, which leads to ±5 meV (±10 meV) changes in the binding energy differences within the considered subset of geometries. Use of a denser ($20 \times 20 \times 1$) mesh with 44 **k**-points in the irreducible wedge resulted in similar variations. Further increasing the potential angular expansion parameter to $l^{\rm pot}_{\rm max} = 6$ and the plane wave cutoff of the potential representation to 256 Ry hardly affected the relative binding energies at all (±3 meV, ±5 meV). A similar result was obtained, when increasing the vacuum region to 19 Å. The error due to the finite slab size is the larger, the more sub-surface oxygen is present in the slab. We repeated all calculations for the (1×1) geometries at 0, 1, and 2 MLs done originally with a six metal layer slab, now using ten metal layer slabs. While the absolute binding energies were lowered by up to 60 meV, the obtained relative differences in $E_{\rm b}(\theta)$ between the different tested geometries were within ±20 meV (±30 meV). Combining all these tests, we can give a conservative estimate of the numerical uncertainty of ±30 meV (±50 meV), when comparing relative binding energies in geometries containing an equal (unequal) amount of O. This inaccuracy never influences the energetic sequence among the structures, i.e. the most stable geometry at one coverage always remains the most stable one, neither does it change the trend of $E_{\rm b}(\theta)$ with coverage. Hence, none of the physical conclusions drawn are affected by the numerical error bars.

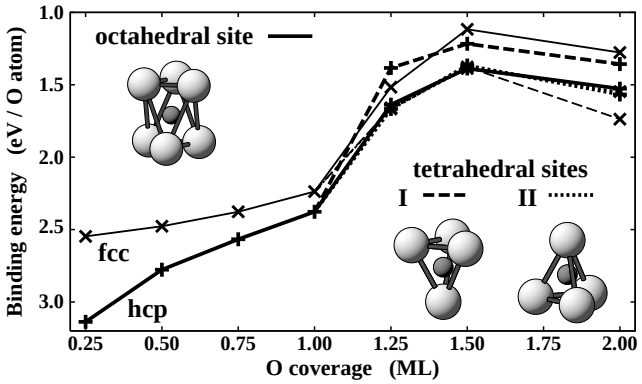

FIG. 1. Binding energies per O atom, $E_{\rm b}(\theta)$, with respect to 1/2 O_2, cf. eq. (1). Coverages with $\theta < 1$ ML correspond to pure on-surface adsorption (hcp or fcc site). For $\theta > 1$ ML an O(1×1) arrangement is always present at the surface, while the remaining O is located in either the octahedral or one of the two tetrahedral sites between the first and second substrate layer. The inserts show the local atomic coordination of each of these sub-surface sites (Ru = light, big spheres, O = dark, small spheres). From the six possible structures at each coverage, the three with the on-surface O in hcp (fcc) sites are drawn with thicker (thinner) lines.

III. RESULTS

A. Oxygen chemisorption and initial incorporation

The initial O chemisorption on the clean Ru(0001) surface proceeds via the formation of four ordered adlayer

phases, in which with increasing coverage oxygen consecutively fills the four available hcp sites inside a (2×2) unit cell[2,9]. Although the calculated binding energy, cf. Fig. 1, decreases markedly during this coverage sequence, $0 < \theta \leq 1\,\mathrm{ML}$, the formation of a complete monolayer on the surface corresponding to the O(1×1)/Ru(0001) phase shown in Fig. 2a is still highly exothermic[8,9]. It is worth mentioning that despite this decrease in the binding energy, the calculated O-Ru bond length remains almost constant, varying only from 2.01 Å in the $O(2 \times 2)$ to 1.97 Å in the $O(1 \times 1)$ phase. We find the available sub-surface sites to be significantly less favourable compared to the on-surface sites, so that we can safely rule out O incorporation into the lattice before the full chemisorbed overlayer is formed[10,12]. A similar conclusion has recently been reached in a thorough experimental study by Böttcher and Niehus[13].

To address the ensuing O penetration into the Ru(0001) surface we first consider all available high-symmetry sub-surface sites between the first and second substrate layer. Namely, these are one octahedral site with sixfold Ru coordination (henceforth referred to as octa) and two tetrahedral sites with fourfold Ru coordination (henceforth referred to as tetra-I and tetra-II). The octa and tetra-I sites are the sites directly below the on-surface fcc and hcp sites respectively, whereas the tetra-II site is located below a surface Ru atom as sketched in Fig. 1. A coverage beyond 1 ML is obtained by combining the $O(1 \times 1)$ adlayer in either hcp or fcc sites with the surplus oxygen in one of the three available sub-surface sites. This results in a total of six possible geometries at each coverage considered. To obtain the trend of $E_\mathrm{b}(\theta)$ in the coverage range $1 < \theta \leq 2\,\mathrm{ML}$ we employ (2×2) unit cells and calculate the binding energy of geometries with one ($\theta = 1.25\,\mathrm{ML}$), two ($\theta = 1.50\,\mathrm{ML}$) and four ($\theta = 2.00\,\mathrm{ML}$) sub-surface oxygens.

The corresponding average binding energies, $E_\mathrm{b}(\theta)$ for $1\,\mathrm{ML} < \theta \leq 2\,\mathrm{ML}$, are markedly lower than the ones in the chemisorption regime for any of the possible site combinations as shown in Fig. 1. This reflects the aforementioned fact, that the now additionally occupied sub-surface sites are considerably less favourable. Nevertheless, all of the structures are still exothermic with respect to clean Ru(0001) and molecular oxygen, and should thus be able to form. Strikingly, $E_\mathrm{b}(\theta)$ for $1\,\mathrm{ML} < \theta \leq 2\,\mathrm{ML}$ does not decrease monotonically with coverage anymore, but shows an inflection, so that the most stable configuration in this coverage range is found for a 2 ML geometry with the on-surface O in fcc and the sub-surface O in tetra-I sites, cf. Fig. 1 and 2c. This implies that it is energetically more favourable to place a given amount of sub-surface oxygens in a finite area at the high local 2 ML coverage into this fcc/tetra-I geometry, rather than to distribute the same number of sub-surface oxygens homogeneously over the surface, where then only the lower binding energy corresponding to the lower local coverage is gained. Contrary to the chemisorption regime, where the decreasing binding energy with coverage indicates

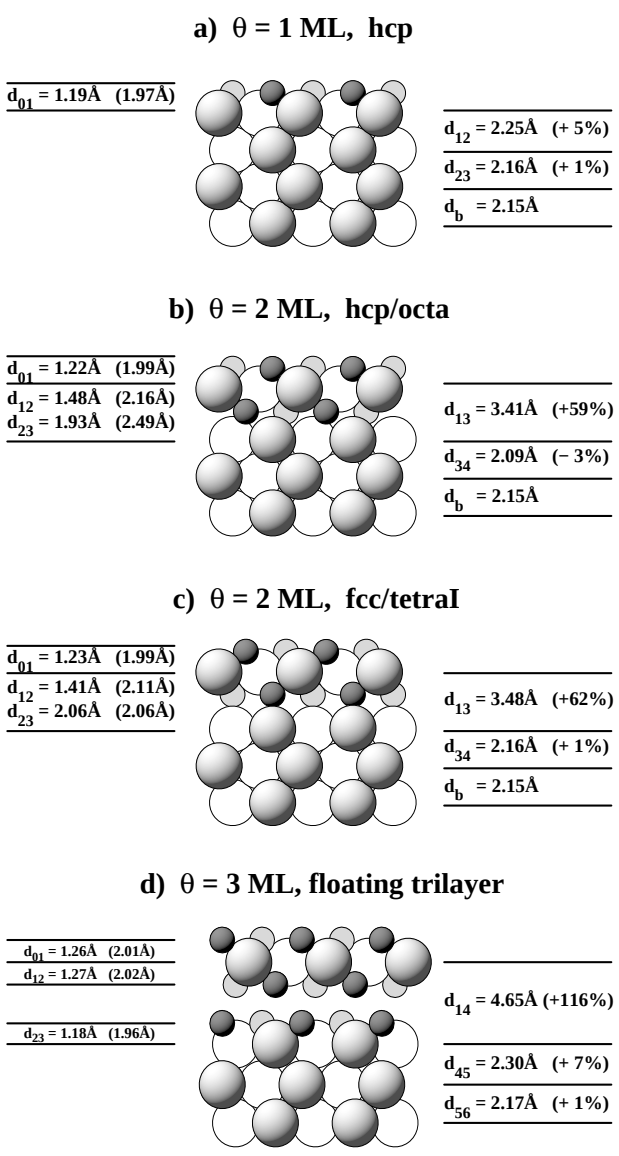

FIG. 2. Sideview of several geometries along the oxidation pathway (see text). Ru = light big spheres, O = dark, small spheres, atoms not lying in the plane itself are white.

that a repulsive interaction between the electronegative adsorbates favours the formation of sparse ordered adlayers, we thus find a tendency for the sub-surface oxygen to accumulate in dense two-dimensional islands with a local (1×1) periodicity. To verify that these islands are indeed two-dimensional, i.e. that the sub-surface oxygen accumulates only between the first and second substrate layer, we additionally calculated a series of geometries, where the coverage between the first and second metal layer was smaller than one and an additional oxygen atom was placed in sites between the second and third metal layer. All of these cases were significantly less stable than the 2 ML fcc/tetra-I geometry, so that we can safely exclude a dendritic 3D growth of the sub-surface O islands into

the substrate.

In these two-dimensional islands, the incorporated oxygen induces a significant distortion of the metal lattice. The first layer distance is expanded by 62% compared to the Ru bulk value, so that instead of an oxygen embedding in the host the geometry is more appropriately described in terms of an O_{ad}-Ru-O_{sub} trilayer on top of a Ru(0001) substrate, cf. Fig. 2c. It is worth mentioning that we find similarly large deformations for all of the tested structures: Even inside the crystal the calculated O-Ru bondlengths are always close to ~ 2.1 Å for O in tetrahedral sites and around 2.2 Å for O in octahedral sites. These optimum bondlengths are incompatible with the available geometric space in the tetrahedral or octahedral interstitial sites of the Ru lattice, which would only allow for bondlengths of 1.65 Å or 1.90 Å respectively. Hence, O incorporation (particularly into the tetrahedral sites) invariably leads to a strong local deformation of the metallic lattice.

As such distortions are easier established at the surface, this would then render oxygen incorporation deeper into the bulk less favourable. Indeed, we find by more than 0.1 eV decreased binding energies at total coverages of $\theta = 1.25$ ML and $\theta = 2.00$ ML, when placing O into the three sub-surface sites between the second and third substrate layer compared to the hitherto discussed incorporation directly below the surface, i.e. between the first and second substrate layer. To address the possibility of bulk dissolved oxygen, we also calculate the binding energy of one O in an octahedral interstitial site in a large $(4 \times 4 \times 4)$ Ru bulk unit-cell with 64 metal atoms, where we allow its nearest Ru neighbours to relax. Due to the finite size of the used supercell, the resulting $E_b = -1.76$ eV does not take the long-range elastic interactions of the metallic lattice properly into account. We estimate that the latter would not improve the binding energy by more than 0.5 eV, so that we may state a conservative upper limit of $E_b \approx -1.25$ eV for the binding energy of bulk dissolved oxygen. Although the latter species is therefore energetically significantly less stable than the afore discussed sub-surface O, just the vast number of available sites might still allow to deposit considerable amounts of oxygen into the sample at finite temperatures. To test this, the concentration, N_O/N_{sites}, of N_O oxygens in the N_{sites} available sites in the crystal can be estimated by minimizing the Gibbs free energy, which leads to[14]

$$\frac{N_O}{N_{sites}} = e^{E_b/k_B T}, \qquad (2)$$

where k_B is the Boltzmann constant. Inserting our upper limit for the binding energy, the concentration would still be as low as 10^{-21} and 10^{-8} at room temperature and $T = 800$ K respectively. As in surface science experiments uptakes are usually quantified in ML, we convert these concentrations by considering a cubic Ru crystal of 1 cm^3 volume. The number of octahedral interstitial sites inside Ru is $7.25 \cdot 10^{22}$ sites/cm^3 and a coverage of 1 ML corresponds to $1.56 \cdot 10^{15}$ atoms/cm^2. Hence, the above stated concentrations would translate into the equivalents of 10^{-14} ML and 0.5 ML at room temperature and $T = 800$ K respectively. From this we conclude, that the total amount of bulk dissolved oxygen in a Ru crystal is completely negligible in the considered temperature range and that incorporated oxygen will predominantly stay as close as possible to the surface.

In conclusion, these results sketch the following picture of the initial oxidation of the Ru(0001) surface: After the completion of a dense O(1×1) adlayer on the surface, subsequent O incorporation occurs preferentially into sites directly below the surface. This sub-surface O accumulates in two-dimensional islands with a local (1×1) periodicity, leading to the formation of an O-Ru-O trilayer on top of the Ru(0001) substrate. In this trilayer, the oxygens occupy fcc and tetra-I sites on and below the surface respectively, in contrast to the coexisting O(1×1) domains, where the on-surface oxygen sits in hcp sites.

B. Trilayer formation and surface registry shift

The already mentioned perception of the geometry in the sub-surface islands as an O_{ad}-Ru-O_{sub} trilayer on top of a Ru(0001) substrate is also what yields to an understanding of the particular stability of the 2 ML fcc/tetra-I structure. Focusing first on the internal trilayer geometry, we notice that only the combinations hcp/octa and fcc/tetra-I lead to O octahedra formed by three on-surface and three sub-surface oxygens surrounding each Ru atom, cf. Fig. 2b and c. This sixfold oxygen coordination of Ru, similar to the situation in the RuO_2 bulk oxide, is energetically preferred to the fourfold coordination with the Ru atoms located in a tetrahedral configuration, present in the two geometries with the sub-surface O in tetra-II positions. Although the two remaining possibilities, fcc/octa and hcp/tetra-I, would also result in a sixfold O coordination of the metal atoms, they are electrostatically considerably less favourable, as there the electronegative on- and sub-surface oxygen atoms sit directly on top of each other at rather close distance.

While the trilayer geometry itself thus favours the hcp/octa and fcc/tetra-I configurations, it is the coupling to the underlying substrate that finally leads to the preference for the latter combination. Actually, the prior geometry is in fact unstable against a registry shift of the whole trilayer along the $[\bar{1}\bar{1}2]$ direction as drawn in Fig. 3. At the end of this barrierless displacement, in which the complete O_{ad}-Ru-O_{sub} film slides over the Ru(0001) surface, the on-surface oxygens are located in fcc and the sub-surface O in tetra-I sites. As both the electronic and the geometric structure within the trilayer are found to remain virtually unchanged during this motion, we attribute the substantial binding energy gain of 0.2 eV per O atom primarily to an improved trilayer-substrate bonding between the sub-surface oxygens and

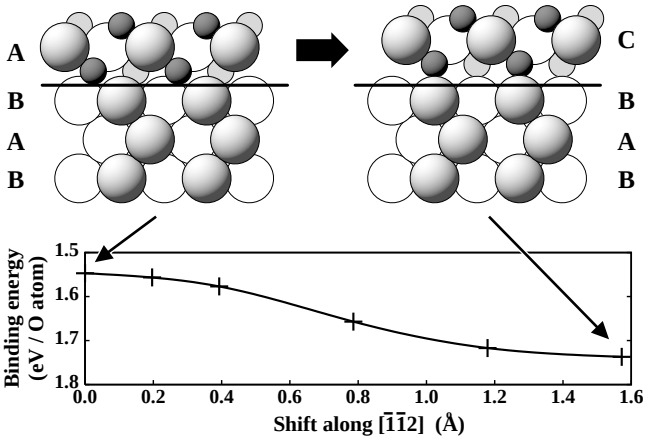

FIG. 3. Atomic geometries and binding energy during the trilayer shift along the [$\bar{1}\bar{1}$2] direction. Starting from the hcp/octahedral configuration (top left), the trilayer slides over the Ru(0001) substrate and ends up in a fcc/tetrahedral-I arrangement (top right), where the first Ru layer lies in a stacking fault position (Ru = light, big spheres, O = dark, small spheres, atoms not lying inside the plane itself are white).

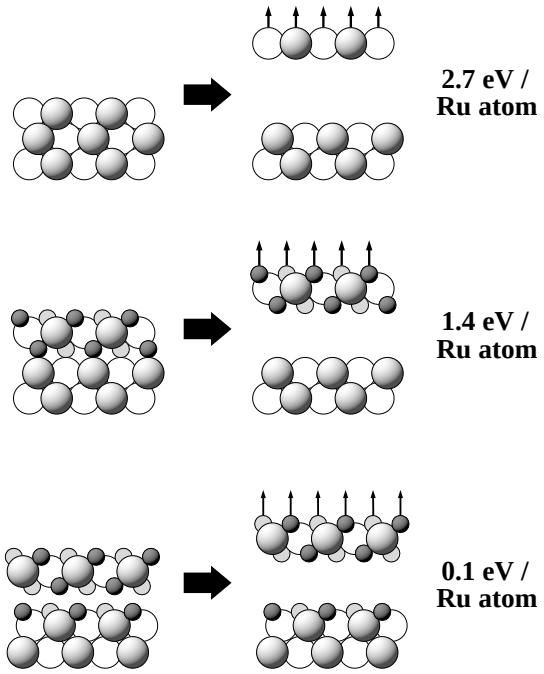

FIG. 4. Energy per Ru atom required to lift off a complete Ru layer from the Ru(0001) substrate. The strong decrease along the sequence clean surface (top panel), 2 ML fcc/tetrahedral-I (middle panel) and 3 ML floating trilayer (bottom panel) indicates a significant destabilization of the Ru(0001) surface upon increasing oxidation.

the topmost Ru atoms of the underlying metal (Ru_{2nd}). This is also corroborated by the outward movement of the latter, such that the corresponding layer distance, d_{34}, relaxes from a clean-surface like -3% contraction in the hcp/octa geometry to a $+1\%$ expansion in the final configuration, cf. Fig. 2b and c.

The only structural difference at the endpoint of the sliding motion compared to the initially tested fcc/tetra-I geometry is that the O-Ru-O trilayer as a whole is rotated by 60^o with respect to the metal below, cf. Fig. 2c and 3. While this leaves both the internal trilayer geometry, as well as the direct coordination of the sub-surface oxygens to its Ru neighbours identical, the first layer Ru atoms now end up in a stacking fault position. We find both fcc/tetra-I geometries to be energetically and electronically degenerate within our calculational uncertainty, so that the first layer Ru atoms (which position with respect to the substrate is the only thing that changes) cannot contribute noticeably to the bonding to the underlying metal anymore. The only remaining coupling film-substrate occurs thus via O_{sub}-Ru_{2nd} bonds, which are strongest in the fcc/tetra-I geometry.

This sliding instability of the hcp/octa configuration also provides a possible mechanism with which the most stable fcc/tetra-I geometry can be realized: At first glance, it appears that kinetics will hinder the formation of the latter, as it seems to imply that all oxygen on-surface adatoms in the $O(1\times1)$ phase, which initially occupy the hcp sites, would have to change their position to fcc upon sub-surface O incorporation. Instead of a collective jump, which would of course be penalized with a high barrier, the penetration process could in reality and at finite temperatures commence with finite-size islands of sub-surface oxygen in all of the available sites (which are energetically not very different). Above a certain critical extension, growing islands with the hcp/octa configuration would then be liable to the sliding motion, once the significant energy gain of 0.2 eV per O atom due to the shift overcomes the cost due to edge effects (which are not considered in our periodic calculations). This mechanism would be particularly facilitated at step edges, where the lateral trilayer shift does not come into conflict with the atoms of the neighbouring domain.

Wrapping up the present argument, we believe that the key feature of our calculations concerning the initial O incorporation into the metal is the formation of two-dimensional (1×1) sub-surface O islands, in which a Ru layer is getting nearly detached from the bulk through the formation of an O_{ad}-Ru-O_{sub} trilayer, which is more strongly bound in itself rather than to the underlying substrate. Although the sliding motion into the fcc/tetra-I geometry helps to enhance this residual coupling of the trilayer to the substrate, it is nevertheless significantly lower than that of the top Ru layer to the substrate in the original pure metal. This is exemplified in Fig. 4, where we compare the energies per (1×1) cell required to completely lift off a metal layer in both cases: The original cost of 2.7 eV per Ru atom to lift off a Ru layer from clean Ru(0001) is almost halved, if the Ru layer is contained inside the O-Ru-O trilayer in the fcc/tetra-I structure (1.4 eV / Ru atom), thus reflecting

a considerable destabilization of the metal surface upon oxidation.

C. Decoupling and continued oxidation

From the understanding of a trilayer formation on top of Ru(0001), we next turn to the question of how this film would continue to grow at higher O coverages. As the lattice deformation cost renders sites closest to the surface most stable and will again favour the formation of dense O(1×1) islands, we address the continued oxidation by directly calculating structures including a total of 3 ML O, i.e. in addition to the hitherto considered (1×1) on- and sub-surface oxygen, we place another ML of O in sites between the second and third substrate layer. Testing all combinations of the two possible on-surface and three possible sub-surface sites totals to 18 trial geometries at this coverage. Strikingly, the most stable geometry corresponds to none of these, but is found, when the additional O ML is also located between the first and second substrate layer, so that both the tetra-I and the tetra-II sites are occupied as shown in Fig. 2d.

Due to the additional sub-surface O, the O-Ru-O trilayer has thus not grown in thickness itself, but has been almost completely decoupled from the underlying Ru metal, as expressed by the tremendous first layer expansion of 116% and the now almost zero binding per Ru atom as shown in Fig. 4[15]. However, one should keep in mind that this virtual decoupling does not mean that the whole trilayer will lift off at finite temperatures: The binding of 0.1 eV/Ru atom scales of course with the large number of Ru atoms in a finite-size island, which would total to a high cost for a complete detachment of the island. Yet, when comparing the binding energies per Ru atom shown in Fig. 4, the pronounced destabilization trend along the oxidation sequence is very clear and should be compared to the significantly lowered emission temperatures of RuO_x fragments from O-rich Ru(0001) surfaces observed in recent temperature desorption spectroscopy (TDS) experiments[16].

With the O-Ru-O trilayer almost decoupled, the underlying substrate will then primarily be influenced by the remaining third oxygen ML sitting in tetra-II sites, i.e. in hcp sites with respect to the second Ru layer. Indeed, when looking at the Ru substrate below the trilayer in more detail, its electronic and geometric structure very much ressembles a O(1×1) covered Ru(0001) surface with 1 ML O in hcp sites, cf. Fig. 2a and d: The trilayer on top has apparently only a negligible influence. Comparing with the fcc/tetra-I configuration at 2 ML coverage, the effect of the additionally incorporated oxygen ML is thus to enable an efficient decoupling of the O-Ru-O film by saturating the underlying substrate bonds.

It it interesting to compare these findings with recently published data on the structure of ultrathin aluminium oxide films on several metallic substrates[17]. In that case a O(1 × 1) layer was also always found to reside below the oxide film and above the underlying metal, at a similar position as in the corresponding chemisorption phase. Hence, the presence of a terminal oxygen layer at the metal-oxide interface (saturating the underlying substrate and in turn minimizing the coupling to the oxide) could in fact be a more general phenomenon.

Given the negligible effect of the floating trilayer on the substrate below, we finally deduce that the continued interaction of oxygen with the Ru(0001) surface will proceed in an analogous fashion as before: In the coverage sequence $3\,\mathrm{ML} < \theta < 4\,\mathrm{ML}$ oxygen will be incorporated below the Ru_{2nd} atoms leading to the formation of a second O-Ru-O trilayer. The latter will then become decoupled by the fifth ML oxygen, after which the next trilayer will be formed, and so on. This way, a stack of weakly coupled trilayers would successively be formed, below which a terminal sub-surface O layer saturates the metal substrate.

D. Accordion effect and transition to the oxide structure

At this point it is natural to ask, whether the formation of the O-Ru-O trilayers wouldn't already correspond to what is often termed a surface oxide. Indeed, the sixfold coordination of Ru in the trilayer together with the correct stoichiometry (one Ru, two O) offers quite some resemblance to the bulk oxide, though one has to concede that the geometry is still distinctly different to the rutile structure of the stable bulk RuO_2.

Experimentally, the end product of the oxidation of the Ru(0001) surface has been convincingly characterized as crystalline, well-oriented $RuO_2(110)$ oxide domains, which are incommensurate to the underlying Ru matrix, but aligned along the three $[\bar{1}\bar{1}2]$ directions on the (0001) basal plane[3]. Hence, we compare in Fig. 5 the structure of our O-Ru-O trilayer with such a (110)-oriented rutile plane. At first glance, both have very little in common and one notices primarily the largely different dimensions of the surface unit cells, which obviously inhibit a commensurate growth of $RuO_2(110)$ on a Ru(0001) substrate. Yet, upon closer inspection it becomes clear, that the trilayer can be transformed rather naturally into $RuO_2(110)$ by a simple accordion-like lateral expansion, involving a tilting of the fixed O octahedra around every second row of Ru atoms as explained in Fig. 5. During this expansion the self-contained trilayer, which offers the preferred sixfold O coordination to every Ru atom, unfolds into a more open geometry, in which every second Ru atom is now only fourfold coordinated, i.e. so-called coordinatively unsaturated (cus) Ru atoms are formed.

Although this accordion-effect offers thus a nice transformation mechanism, without any material transport apart from mere expansion, it is not immediately clear,

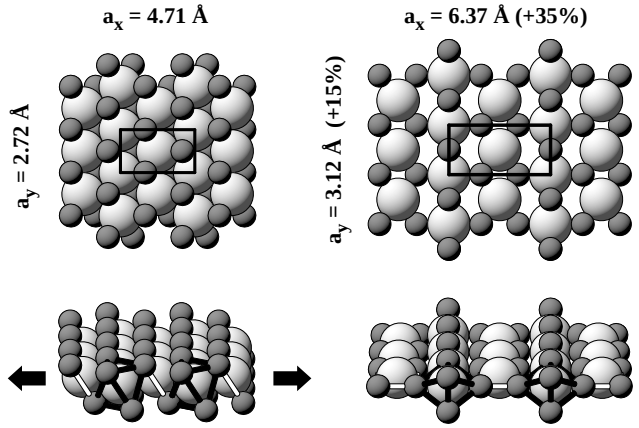

FIG. 5. Atomic geometries of the O-Ru-O trilayer (left) and a RuO_2(110) rutile layer (right). The top panels show a top view, comparing the surface unit cells. The bottom panels depict a perspective view, where O coordination octahedra are drawn around the metal atoms. The trilayer can be transformed into the rutile geometry by a lateral expansion (along the arrows), keeping the drawn O-O bonds (white and black lines) rigid. This way an alternating sequence of fully coordinated Ru atoms (inside the tilted octahedra, black bonds) and coordinatively unsaturated (cus) Ru atoms (surrounded by only four O atoms, white bonds) is created.

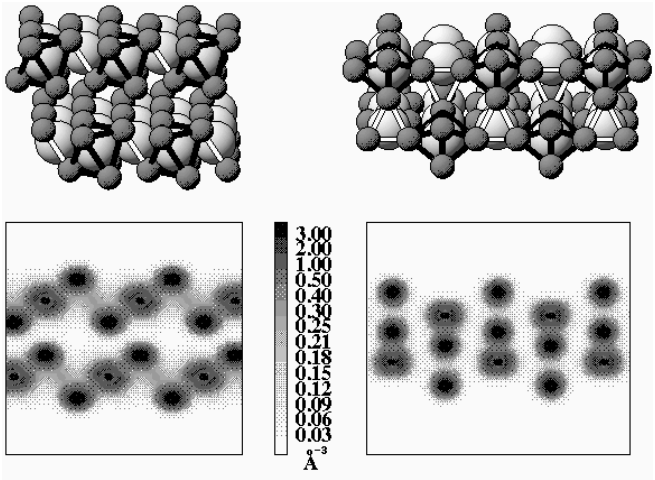

FIG. 6. Comparison of the inter-trilayer bonding of the O-Ru-O trilayer (left) and of RuO_2(110) rutile layers (right): perspective view of the atomic geometry (top panels) and calculated electron density perpendicular through the slabs along the $[\bar{1}\bar{1}2]$ direction (bottom panels).

what would drive the self-contained trilayer into such a much more open and coordinatively less favourable geometry. And in fact, the key behind the transition becomes only apparent, when considering higher film thicknesses: Whereas before the expansion two trilayers are found to bind only negligibly to each other (which is comprehensible, given that each trilayer alone already offers a bulk oxide-like coordination to the metal atoms), a stacking of rutile layers increases the local coordination of the cus Ru

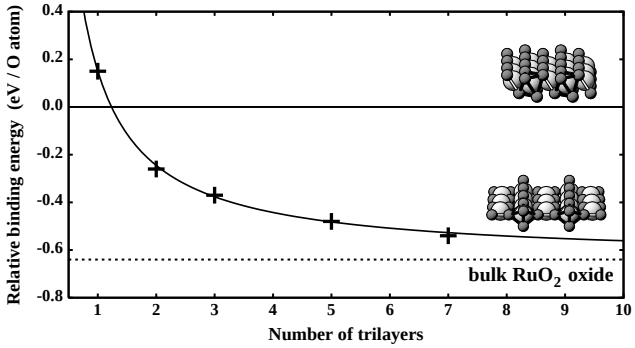

FIG. 7. Relative binding energy difference between a stack of O-Ru-O trilayers and of RuO_2(110) rutile layers as a function of layers in the stack. The negligible intertrilayer bonding in the former case leads to a constant binding energy per O atom, which is taken as the zero reference. Due to the formation of new bonds the average binding energy per O atom increases in the rutile case, rendering this structure energetically more favourable than the O-Ru-O trilayers as soon as two trilayers are packed onto each other. Additionally drawn is the average binding energy in an infinite bulk RuO_2(110) arrangement (dotted line), which is the limit approached by the rutile curve for thicker slabs.

atoms by the bridging O atoms of the next layer, thus retrieving the ideal sixfold coordination for all metal atoms as shown in Fig. 6.

Precisely this additional inter-layer coordination in the rutile case eventually leads to a stabilization of this structure for higher film thicknesses. To this end, we compare in Fig. 7 the relative binding energies of a stack of trilayers with a corresponding stack of rutile layers, where we neglect for the time being any residual influence of the underlying Ru substrate. As the O-Ru-O trilayers hardly bind to each other, the binding energy turns out independent of the number of trilayers stacked onto each other. On the contrary, the more rutile layers one packs together, the more the average binding energy increases, indicating that the increased coordination of the cus Ru atoms indeed leads to the formation of inter-layer bonds. While one isolated O-Ru-O trilayer is still by 0.15 eV per O atom more stable than its more open rutile counterpart, this situation reverses already as soon as two trilayers are packed onto each other. For thick rutile films, the binding energy finally approaches gradually the limit, by which bulk rutile RuO_2 is more stable than an infinite stack of O-Ru-O trilayers, namely by 0.64 eV per O atom, cf. Fig. 7.

Based on this comparison, we would hence estimate a phase transition into a RuO_2(110) oxide film after two or more O-Ru-O trilayers have formed during the oxidation. Yet, we notice that in this energetic comparison, the residual influence of the underlying metal has been neglected. While we have shown that this interaction is negligible in the O-Ru-O trilayer case, cf. Fig. 4, this is not so clear for the incommensurable rutile lay-

ers on Ru(0001). However, the exact value of this interaction, which is limited to the atoms directly at the interface, is not really relevant, as it will certainly not prevent the transition to the rutile structure for thicker films, where the binding energy gain scales with the number of inter-layer bonds formed throughout the whole film. Independent of the interaction with the underlying metal substrate, the film will therefore switch to the rutile structure once a critical film thickness is exceeded, which concludes our suggested oxidation pathway. The involved accordion-like unfolding of the trilayers leads then rather naturally to $RuO_2(110)$ oriented domains, which are due to the large lateral expansion incommensurate, but aligned to Ru(0001), in agreement with the experimental data[3].

In this respect it is interesting to notice that the calculated energetic difference between such ultrathin RuO_2 films and the intermediate precursor configurations along the oxidation pathway is not large. At elevated pressures and temperatures a lively dynamics between these metastable configurations is therefore conceivable, which would of course affect the chemical and mechanical properties of the surface. In the case of Ru, it was already shown that contrary to common believe the oxidic domains, which evolve on the surface in the reactive environment, form an essential ingredient to understand the catalytic activity[3,18]. Yet, our findings suggest that the situation might be even more complex, requiring possibly also an inclusion of the dynamics between various metastable configurations to achieve a reliable molecular-level description of the catalytic reaction. To verify this for the particular case of Ru and other metals (where we expect an analogous situation), experimental studies addressing the microscopic structure of surfaces in realistic environments (and/or under steady-state reaction conditions) are obviously mandatory.

E. Searching for the precursor

As apparent from the preceding Sections, the salient feature of our suggested oxidation pathway is the formation of an O-Ru-O trilayer on top of Ru(0001) as a metastable precursor to the final oxide film. Up to now, there is no direct experimental evidence for this trilayer, which we attribute to the fact, that all studies addressing the oxidation of the Ru(0001) surface have hitherto unanimously employed rather elevated temperatures, which in turn enable a rapid phase transition to the final RuO_2 bulk oxide structure. While it is presently not clear, whether it will at all be feasable to stabilize the trilayer by gently oxidizing the Ru(0001) surface at sufficiently low temperatures, we still hope that our results may inspire carefully directed experiments by listing in the following a number of observables that might be used as a fingerprint.

Along our suggested oxidation pathway, the O-Ru-O trilayer occurs in three different positions with respect to the underlying metal substrate: first in a hcp/octa configuration, then in a fcc/tetra-I geometry after the surface registry shift and finally decoupled by the third incorporated O layer. From a structural point of view, all three precursor geometries are laterally still commensurate to the underlying Ru(0001). It is only the significant expansion during the accordion-unfolding that finally leads to the distinctly different $RuO_2(110)$ lattice spacing of the oxide domains. Just up to this last transition, the surface should therefore only exhibit the hexagonal (1×1) low energy electron diffraction (LEED) pattern corresponding to the basal Ru(0001) plane. Whether or not the trilayer has switched to the final rutile structure can therefore easily be monitored by the appearance of new LEED spots, which due to the incommensurability of both lattices show up at completely different positions on the screen[19]. Samples, for which TDS curves tell that more than one oxygen ML have been deposited and for which a sharp (1×1) LEED pattern without extra spots is observed, are therefore most likely candidates for sub-surface oxygen.

If such a preparation has led to the formation of (1×1) sub-surface islands, could then be visible in scanning tunneling microscopy (STM) experiments: The sub-surface oxygen induced vertical relaxations are huge, cf. Fig. 2, and should enable an identification of the corresponding islands in the STM images. With respect to the surface registry shift, it would be particularly interesting to check whether the atomic lines in the (1×1) periodic islands are still in registry with the surrounding domains across the island perimeter: After the surface registry shift, the on-surface oxygens in the island will be in fcc positions in contrast to the hcp site in the neighbouring $O(1\times1)$ domains, which should correspondingly show up in an STM image. Of course, the largely different layer distances in the sub-surface patches will also lead to distinctly different LEED I(V) curves, which could therefore also be used for fingerprinting. Even with only poorly defined long range order on the surface, the significantly increased Ru-Ru bondlengths between the metal atoms in the trilayer and the metal atoms of the underlying substrate might still show up in extended x-ray absorption fine structure (EXAFS) data.

In Fig. 8 we show the computed workfunctions, Φ, for the geometries along the oxidation sequence. Up to the completion of the full (1×1) on-surface adlayer, Φ rises continuously, which has been explained in terms of the increasing dipole moment due to the chemisorbed oxygen[9]. Interestingly and contrary to common believe, we find that the incorporation of O into the sub-surface region does not cause an analogous reduction of the workfunction due to the build-up of a now inverted dipole moment. Instead, Φ continues to rise inside the (1×1) islands, until it reaches a very high value of 7.53 eV for the floating trilayer structure. In Fig. 8 we also included the workfunctions for the two possible surface terminations of the final $RuO_2(110)$ oxide domains[20,21]: In addition to the

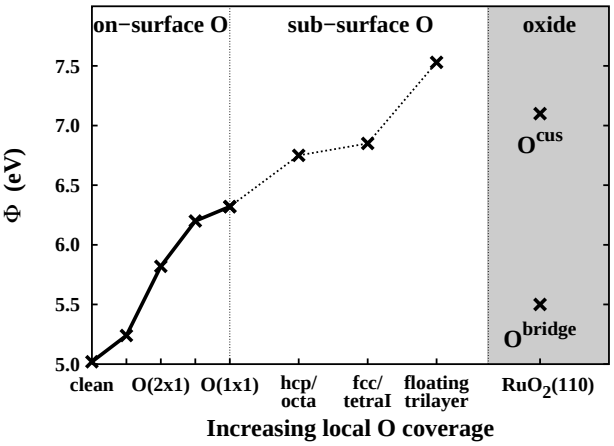

FIG. 8. Calculated workfunction, Φ, along the oxidation pathway. The work-function rises throughout the on-surface chemisorption of O at $0 < \theta \leq 1$ ML, but is even increased at the three metastable precursor configurations, cf. Fig. 2. For comparison also the calculated workfunction of the two possible terminations of $RuO_2(110)$ domains is shown. The latter oxidation stage (in the grey shaded area) should be clearly distinguishable from the sub-surface O precursors by the appearance of new LEED spots as described in the text.

traditionally conceived stoichiometric rutile(110) termination, O^{bridge}, oxygen-rich conditions can further stabilize a so-called polar termination, O^{cus}, with excess terminal O atoms, which lead to a significantly higher work function compared to the stoichiometic case[21]. In light of the results shown in Fig. 8, we argue that the decrease in the workfunction upon oxidation reported by Böttcher and Niehus[13] (which was then attributed to the presence of sub-surface oxygen) in fact reflected already the gradual formation of O^{bridge} oxide domains on the surface, whereas sub-surface oxygen would in reality lead to increasing workfunctions. Note, that the oxide formation goes hand in hand with the aforementioned appearance of new LEED spots, so that a high workfunction due to the formation of O^{cus} terminated domains under oxygen-rich preparation conditions should still be clearly distinguishable from a high workfunction due to the floating trilayer. Concomitantly, we suggest that an increasing work function for coverages $\Theta > 1$ ML without the appearance of new LEED spots would represent a likely (yet rather ambiguous) fingerprint for the O-Ru-O trilayer. To better take the heterogeneity of a surface, which includes sub-surface O islands, into account, we therefore believe photoemission of adsorbed xenon (PAX) experiments measuring the local workfunction to be a more suitable technique.

Although X-ray Photoemission Spectroscopy (XPS) is in principle also a most eligible tool to study the oxidation of metal surfaces, we unfortunately find in the present case that it would not lead to a clearcut signal, allowing to identify the precursor geometries. In a recent publication, we have described that in the sequence of ordered adlayers the Ru $3d$ level shifts by up to 1 eV towards higher binding energies, while the O $1s$ level remains almost unchanged[23]. In contrast, the formation of the oxide domains is then characterized by only a small back shift of the Ru $3d$ core level towards lower binding energies compared to its position in the coexisting $O(1 \times 1)/Ru(0001)$ phase, while it is now the O $1s$ which largely shifts in the same direction[24]. To assess the XPS signal received from the possible intermediate precursors, we calculated all Ru $3d$ and O $1s$ surface core level shifts (SCLS) for the hcp/octa, fcc/tetra-I and floating trilayer geometries inside the sub-surface O islands, cf. Fig. 2, using exactly the methodology described in detail in refs. 23,24. Unfortunately, the Ru $3d$ levels in all three structures turn out to lie very close to the position in the coexisting $O(1 \times 1)/Ru(0001)$ phase, so that the incorporation of sub-surface O would not lead to an unambiguously identifyable new signal, but at best to a small shoulder aside an existing peak. This situation is different for the O $1s$ levels, which particularly for the floating trilayer are shifted by 1.1 eV towards lower binding energy compared to the position in the chemisorption phases. However, there they almost coincide with the O $1s$ levels of the $RuO_2(110)$ domains[24], so that the presence of such a peak would only be a clear fingerprint for the sub-surface precursor, if one can safely rule out that no oxide domains have been formed yet.

This ambiguous situation between precursor and final oxide structure is similar in the case of ultraviolet photoemission spectroscopy (UPS). There the disappearance of a broad feature at about -2.5 eV with respect to the Fermi-energy, E_F, was suggested as a marker for the oxidation of the Ru(0001) surface[22]. Well aware of the fact, that calculated densities of states (DOS) can only cautiously be used to interpret UPS data, we show in Fig. 9 how this quantity evolves for the first layer Ru atoms (which would contribute most to the UPS signal) along the oxidation pathway. The DOS for the clean surface shows the Ru $4d$ band, which is slightly narrower than the bulk band due to the lowered coordination of the surface atoms[23] and which is dominated by a peak at -2.0 eV. Analyzing the electron density distribution of the states that contribute to this peak, we deduce that the latter is due to backbonding states to the second substrate layer. The formation of chemisorption states at the edges of the $4d$ band can clearly be seen in the DOS of the $O(1 \times 1)$ on-surface phase and goes hand in hand with a reduction of the feature around -2.0 eV, which according to the electron density distribution analysis is still due to backbonding states to the second layer. The depletion of such states agrees well with the 5% expansion of the first layer distance upon O adsorption as shown in Fig. 2a. We notice in passing, that the bonding oxygen-induced states at the bottom of the band are split into two peaks due to the different lateral interaction of states of p_x/p_y and p_z symmetry within the densely packed O overlayer. Addressing next the DOS of the floating trilayer precursor shown in Fig. 2d, we find now almost no states left at

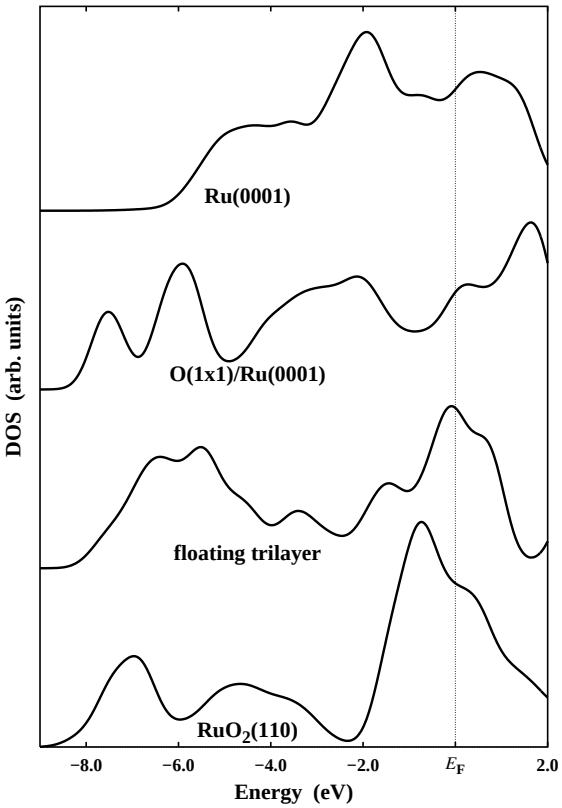

FIG. 9. Calculated 4*d* DOS of first layer Ru atoms in various geometries along the oxidation pathway. The DOS of the first layer Ru atoms in the hcp/octa and fcc/tetra-I positions of the O-Ru-O trilayer (not shown) are very similar to the one shown here, where the trilayer is already almost decoupled from the underlying Ru(0001) substrate at a coverage of $\theta = 3$ ML. The curves have been shifted and strongly smoothed for clarity.

the energies around -4.0 to -2.0 eV reflecting the fact, that the floating trilayer has virtually no Ru-Ru backbonding to the underlying substrate anymore. Continuing to the DOS of the $RuO_2(110)$ domains, this lack of direct Ru-Ru bonds in the oxide leads similarly to few states around this energy region. Instead, the predominant features appear now at -7.0 to -4.0 eV due to O $2p$ - Ru bonding states and slightly below the Fermi level[25]. Based on these results, we suggest that the depletion of the UPS feature around -2.5 eV, which had been suggested as an oxidation marker, simply indicates the diminishing Ru-Ru backbonds at the oxidizing surface, but would not allow to distinguish between the intermediate precursor and the final oxide domains.

IV. SUMMARY

In conclusion, we have presented an atomistic pathway leading from a clean Ru(0001) surface to the $RuO_2(110)$ domains, that were experimentally reported as the end product of the oxidation of this Ru surface. Oxygen penetration into the lattice starts only after the full chemisorbed adlayer is completed on the surface. The ensuing oxygen incorporation leads to the formation of two-dimensional sub-surface O islands between the first and second metal layer, in which an O-Ru-O trilayer gets decoupled from the underlying substrate. Continued oxidation successively leads to the formation of a stack of such trilayers, which finally unfold into the $RuO_2(110)$ oxide structure once a critical film thickness is exceeded.

The salient feature of this suggested oxidation pathway is a floating O-Ru-O trilayer as a metastable precursor to the final oxide film. Detailed structural and electronic data characteristic of this precursor was given in order to inspire and enable a directed experimental search for it at low oxidation temperatures. The large lattice relaxations induced by the sub-surface oxygen render structural techniques like STM, LEED and EXAFS as most promising techniques for such a search, while the precursor would not lead to clearcut fingerprints in XPS and UPS data. A rising workfunction beyond the completion of the adlayer together with a (1×1) LEED pattern would be a positive signal for the predicted intermediate, where particularly PAX measurements of the local workfunction would be ideally suited to take the heterogeneity of the oxidized surface into account. We find all intermediate precursors along the oxidation pathway to be rather close in energy to the final oxide structure, which indicates a likely lively dynamics between the metastable configurations under realistic conditions and which might affect the chemical and mechanical properties of the surface.

ACKNOWLEDGEMENTS

We gratefully acknowledge stimulating discussions concerning the experimental studies on oxidized Ru(0001) with A. Böttcher, B. Krenzer, R. Blume and H. Conrad. This work was partially supported by the Deutsche Forschungsgemeinschaft (Schwerpunkt "Katalyse").

[1] K. Reuter, C. Stampfl, M.V. Ganduglia-Pirovano, and M. Scheffler, Chem. Phys. Lett. (*submitted*).
[2] D. Menzel, Surf. Rev. Lett. **6**, 835 (1999).
[3] H. Over, Y.D. Kim, A.P. Seitsonen, S. Wendt, E. Lundgren, M. Schmid, P. Varga, A. Morgante, and G. Ertl, Science **287**, 1474 (2000).
[4] J.P. Perdew, K. Burke and M. Ernzerhof, Phys. Rev. Lett. **77**, 3865 (1996).
[5] P. Blaha, K. Schwarz and J. Luitz, **WIEN97**, *A Full Potential Linearized Augmented Plane Wave Package for Calculating Crystal Properties*, Karlheinz Schwarz, Techn. Universität Wien, Austria, (1999). ISBN 3-9501031-0-4.

[6] B. Kohler, S. Wilke, M. Scheffler, R. Kouba, and C. Ambrosch-Draxl, Comput. Phys. Commun. **94**, 31 (1996).
[7] M. Petersen, F. Wagner, L. Hufnagel, M. Scheffler, P. Blaha, and K. Schwarz, Comp. Phys. Commun. **126**, 294 (2000).
[8] C. Stampfl, S. Schwegmann, H. Over, M. Scheffler, and G. Ertl, Phys. Rev. Lett. **77**, 3371 (1996).
[9] C. Stampfl and M. Scheffler, Phys. Rev. B **54**, 2868 (1996).
[10] C. Stampfl, H.J. Kreuzer, S.H. Payne, and M. Scheffler, Appl. Phys. A **69**, 471 (1999).
[11] M.V. Ganduglia-Pirovano and M. Scheffler, Phys. Rev. B **59**, 15533 (1999).
[12] M. Todorova, W.X. Li, M.V. Ganduglia-Pirovano, C. Stampfl, K. Reuter, and M. Scheffler, (*in preparation*).
[13] A. Böttcher and H. Niehus, J. Chem. Phys. **110**, 3186 (1999).
[14] N.W. Ashcroft and N.D. Mermin, *Solid State Physics*, Holt-Saunders Int. Ed., Philadelphia (1976).
[15] Note, that due to the negligible coupling of the trilayer to the underlying substrate, it is irrelevant whether we put it in a stacking fault geometry or not: both cases are electronically, structurally and energetically absolutely degenerate.
[16] A. Böttcher, H. Conrad, and H. Niehus, J. Chem. Phys. **112**, 4779 (2000).
[17] D.R. Jennison, C. Verdozzi, P.A. Schultz, and M.P. Sears, Phys. Rev. B **59**, R15605 (1999).
[18] A. Böttcher, H. Niehus, S. Schwegmann, H. Over, and G. Ertl, J. Phys. Chem. B **101**, 11185 (1997).
[19] Y.D. Kim, A.P. Seitsonen, and H. Over, Surf. Sci. **465**, 1 (2000).
[20] Y.D. Kim, A.P. Seitsonen, S. Wendt, J. Wang, C. Fan, K. Jacobi, H. Over, and G. Ertl, J. Phys. Chem. **105**, 3752 (2001).
[21] K. Reuter and M. Scheffler, Phys. Rev. B (*submitted*).
[22] A. Böttcher and H. Niehus, Phys. Rev. B **60**, 14396 (1999).
[23] S. Lizzit, A. Baraldi, A. Groso, K. Reuter, M.V. Ganduglia-Pirovano, C. Stampfl, M. Scheffler, M. Stichler, C. Keller, W. Wurth, and D. Menzel, Phys. Rev. B **63**, 205419 (2001).
[24] K. Reuter and M. Scheffler, Surf. Sci. **490**, 20 (2001).
[25] P.I. Sorantin and K.H. Schwarz, Inorg. Chem. **31**, 567 (1992).